https://doi.org/10.5194/esurf-2021-89
Preprint. Discussion started: 8 December 2021

Earth Surface Dynamics Discussions
Open Access
EGU

Landscape responses to dynamic topography and climate change on the South African source-to-sink system since the Oligocene.

Claire A. Mallard[1], Tristan Salles[1]

[1] School of Geosciences, the University of Sydney, Australia

Correspondence to: Claire A. Mallard (claire.mallard@sydney.edu.au)

Abstract. The South African landscape displays important lithological and topographical heterogeneities between the eastern, western margins and the plateau. Yet the underlying mechanisms and timings responsible for this peculiar layout remain unclear. While studies have proposed a post-Gondwana uplift driver, others have related these heterogeneities to a more recent evolution induced by deep mantle flow dynamics during the last 30 million years. This theory seems supported by the rapid increase of sediment flux in the Orange basin since the Oligocene. However, the triggers and responses of the South African landscape to dynamic topography are still debated. Here we use a series of numerical simulations forced with Earth data to evaluate the contribution of dynamic topography and precipitation on the Orange river source-to-sink system since the Oligocene. We show that, if the tested uplift histories influence deposits distribution and thicknesses in the Orange sedimentary basin, they poorly affect the large-scale drainage system organisation and only strongly impact the erosion across the catchment for two of the four tested dynamic topography cases. Conversely, it appears that paleo-rainfall regimes are the major forcing mechanism that drives the recent increase of sediment flux in the Orange basin. From our simulations, we find that climate strongly smoothed the dynamic topography signal in the South African landscape and that none of the currently proposed dynamic topography scenarios produce an uplift high enough to drive the pulse of erosion and associated sedimentation observed during the Palaeocene. These findings support the hypothesis of a pre-Oligocene uplift. Our results are crucial to improve our understanding of the recent evolution of the South African landscape.

1 Introduction

Conflicting timings and drivers have been proposed to explain the singular South African tilted topography as well as the subsequent increase of the sediment flux in the Orange basin over the last 30 Ma. Previous studies proposed dynamic topography uplifts associated with the African superplume (Lithgow-Bertelloni & Silver, 1998, Gurnis et al., 2000; Nyblade and Sleep, 2003, Braun et al., 2014), with the African plate motion (Burke, 1996; Burke & Gunnell, 2008) or induced by lithospheric heating (Tinker et al., 2008b; Stanley et al., 2013) to explain both the landscape and the sedimentation history of the region. If the underlying mechanisms are still under discussion, the timings and number of uplifts remain also highly debated. Thermochronological data (Brown et al., 1990; Gallagher & Brown, 1999a; Brown et al., 2002, Tinker et al., 2008b; Flowers and Schoene, 2010, Wildman et al., 2015, 2016) and proposed rift models (Gilchrist et al., 1994), are in favour of an early uplift phase (around 130 Ma) induced by thermal uplift and rift inherited topography. Other thermochronological studies combined with increasing sedimentary flux estimates of the Orange and southern sedimentary basins (Tinker et al., 2008a, Rouby et al., 2009, Guillocheau et al., 2012, Baby et al., 2018;2020) support a significant and rapid phase of erosion affecting a large area of the South African plateau in the mid-Late Cretaceous (around 100–60 Ma). The two main proposed mechanisms behind this major pulse of erosion are attributed to 1) a renewal of dynamic topography uplift induced by the LLSVP (Braun et al., 2014) or 2) changes in lithospheric buoyancy (Tinker et al., 2008b, Stanley et al., 2013, Hu et al., 2018).

https://doi.org/10.5194/esurf-2021-89
Preprint. Discussion started: 8 December 2021

Here, we focus on new studies that show a pulse of sedimentation in the Orange basin over the last 25 Ma (Baby et al., 2018, 2020) combined with drainage studies (Roberts & White, 2010, Paul et al., 2014), geomorphological features (Dauteuil et al., 2015), and thermochronology data (Green et al., 2017) which uphold a late Cenozoic uplift. These studies link the last increase of sedimentary flux with either dynamic topography associated with LLSVP (Gurnis et al., 2000) or small-scale convection (Burke, 2008). If some authors suggest that the Cenozoic uplift is directly caused by mantle plume upwelling, others argue that the associated dynamic topography amplitude would be too low (less than 10 m/Myr; Gurnis et al., 2000) and happened too early (South Africa was over the superplume about 70 Ma ago) to justify the rapid erosion of the plateau (Braun et al., 2014).

Various mantle flow models and associated dynamic topography scenarios have been published recently. In this study, we quantify the impact of four dynamic topography scenarios on the Orange River source-to-sink system in order to evaluate its most recent phase of denudation (Partridge and Maud, 1987). These uplifts histories account for different mechanisms: 1- the drift of South Africa over a mantle upwelling inducing a small and 2- long-wavelength uplift (Gurnis et al., 2000, Cao et al., 2019), 3- or inducing a higher and narrower uplift (Hassan 2020) and 4- a tilted east-west uplift induced by the passive north-eastward motion of Africa over a buoyant mantle (Moucha et al., 2011, Braun et al., 2014).

We decided to integrate but not to test various flexural uplifts as we consider that during the last 30 Myrs, the denudation and large volume of sediment shed from the continent (up to 1-2 km for Braun et al., 2014 and up to 1 km for this study) is more likely to be driven by the increase of precipitation than associated with flexural uplift.

Besides dynamic topography, we also explore the role of precipitation as a driver of increasing sediment flux supported by Baby et al., 2018 and 2020. Despite the lack of climate synthesis in the region, we used a compilation of paleo precipitation indicators (Appendix A) to define three paleoclimate maps accounting for spatial and temporal rainfall changes. We did not use climate models; their spatial resolution is too low compared to the 5 km resolution of the landscape used and does not have the same reconstruction as the ones used in the mantle flow simulations. We defined a first episode (Fig. A1a), from 30 to 20 Ma of semi-arid to arid conditions based on Macgregor 2010, 2013. The second episode (Fig. A1b), from 20 to 15 Ma, integrates the observations from Pickford and Senut, 1999, Braun 2014, Salman & Abdula 1995, which results: 1) in increased pluvial stage in the actual Namib desert and 2) a sub humid area in the southern part of South Africa during the Burdigalian (Appendix A). The last episode (Fig. A4), from 15 to 0 Ma, is based on the present-day rainfall record (Burke and Gunnell 2008).

We then evaluate the role of different uplift and climatic histories using the landscape evolution models Badlands (Salles et al., 2016, 2018, Appendix A). Our study tests the most plausible drivers affecting the Orange source to sink system by combining Earth data and numerical models. In our simulations, we account for dynamic topography impact, climate change, sea-level variations (Hacq et al., 1987) (Table A1) as well as spatially variable erodibilities to reflect surface lithologies of the region (Appendix A; Table A2; Fig. A2). Simulation results are then compared to unravel their individual contributions on 1-

https://doi.org/10.5194/esurf-2021-89
Preprint. Discussion started: 8 December 2021

present-day topography of the South African plateau, 2- on the Orange River drainage pattern and 3- on the Orange basin sedimentation over the last 30 Ma.

2 Mantle dynamics

2.1 Mantle convection models

The tested dynamic topography scenarios capture different wavelengths of mantle flow as they are generated with four different methods (Table A1). The dynamic topography estimations of the model M1 results from a global seismic tomography-based backward-forward adjoined model under Boussinesq approximation and is calculated using CitcomS mantle convection model (Liu and Gurnis 2008, Muller et al., 2018). The scenarios AY18 and M2 are also derived from CitcomS mantle flow calculations under the extended Boussinesq approximation (Zhong, 2006) and are driven by plate reconstruction, subduction history and basal heating (Cao et al., 2019, Hassan et al., 2020). The dynamic topography values of the models M1, M2 and AY18 are calculated by removing the first 250 km (Muller et al., 2018; Cao et al., 2019; Hassan et al., 2020) of the upper mantle. The last scenario, model TX08, is extracted from a global joint inversion of seismic and geodynamic data model, which better simulates horizontal velocities and captures higher resolution of mantle flow structures (Forte et al., 2010, Moucha & Forte 2011). These four models have been chosen as they contain dense material similar to present-day Large low-shear-velocity provinces which are impacting the African plate.

2.2 Dynamic topography changes

Model AY18 has an increasing and homogeneous dynamic topography variation for both the Orange river mouth and the plateau (Fig. 1 - blue lines). Model M1 partially captures the mantle anomalies below South Africa as it only resolves large scale mantle structures (>1000 km). In this model, the variations of dynamic topography (Fig. 1 - red lines) results in 50 m subsidence of the Orange river mouth and 50 m uplift of the Drakensberg. Model M2 shows a more complex history with changes in dynamic topography below the Orange River mouth around -100 m over the 30 Ma timeframe while the variations below the Drackensberg are relatively stable over the first 20 Ma before subsiding by -100m during the last 10 Ma (Fig. 1 - grey lines). Model TX08 has the most increasing dynamic topography variations for the period considered. Below the Drakensberg, dynamic topography changes from up to -600 m over the last 30 Myr while the Orange river mouth subsides by 150 m (Fig. 1 - yellow lines).

https://doi.org/10.5194/esurf-2021-89
Preprint. Discussion started: 8 December 2021

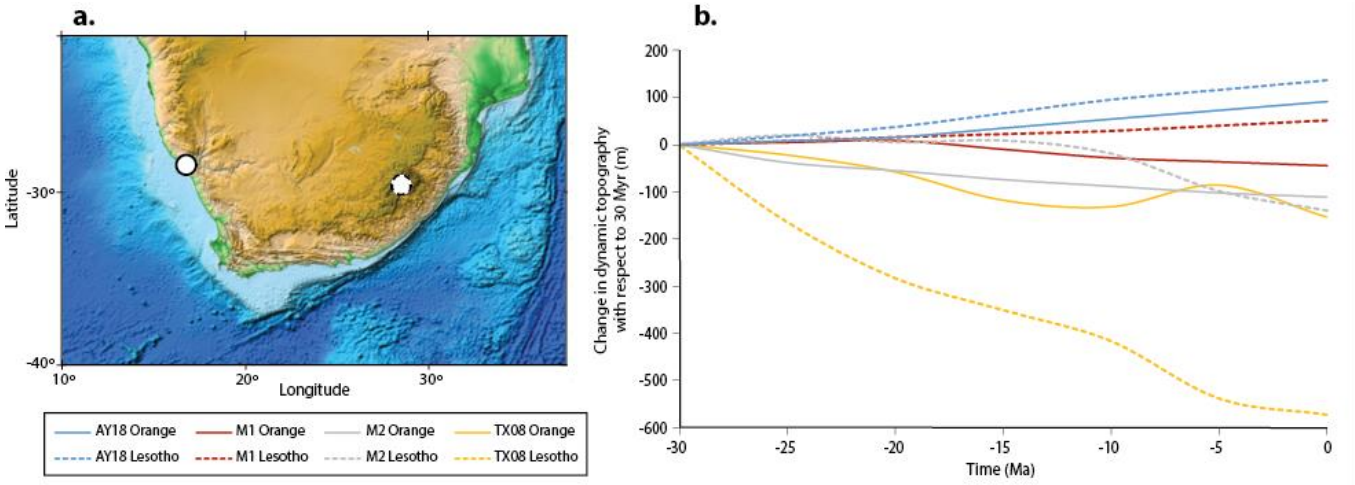

Figure 1: Dynamic topography variations over the last 30 Ma a. Present day topography (NOAA) showing the location of the study area, the Orange river mouth (white circle) and the Drackensberg high (white circle with dashed edges) are used to extract the dynamic topography changes in the right panel. b. Evolution of the South African dynamic topography signal at the Orange river mouth (straight lines) and the Lesotho (dashed lines) over the last 30 Myr for the four tested models: AY18 in blue, M1 in red, M2 in grey and TX08 in yellow.

3 Landscape evolution models

3.1 Building the initial paleo-elevations

Considering that the tectonic history of South Africa was quiet during the Oligocene, we choose to generate the initial paleo-elevation of the landscape evolution model by inverting the dynamic topography histories presented in Fig. 1. We extract this signal and subtract it from the actual topography model ETOPO1 (NOAA). We also remove the estimated load of sediments for the last 30 Ma as well as the associated isostasy component (Appendix A; Fig. A3, Table A1). We did not add the volume of eroded sediments (i.e., sediments accumulated on the margins) in the Orange catchment basin as we consider that 1) the volume of eroded material vs. the area of the catchment basin is small (2000 km wide with an extent of more than 5.e5 km^2), 2) the source system is poorly constrained and 3) our study focuses on rates of sediment fluxes changes more than on their specific values. We recognise that this bias will lower the present-day topography of the primary source areas as well as lower the resulting marine deposit thicknesses. Despite this limitation, this approach produces for each mantle dynamic histories a corresponding high-resolution paleo-elevation maps (Fig.2a).

https://doi.org/10.5194/esurf-2021-89
Preprint. Discussion started: 8 December 2021

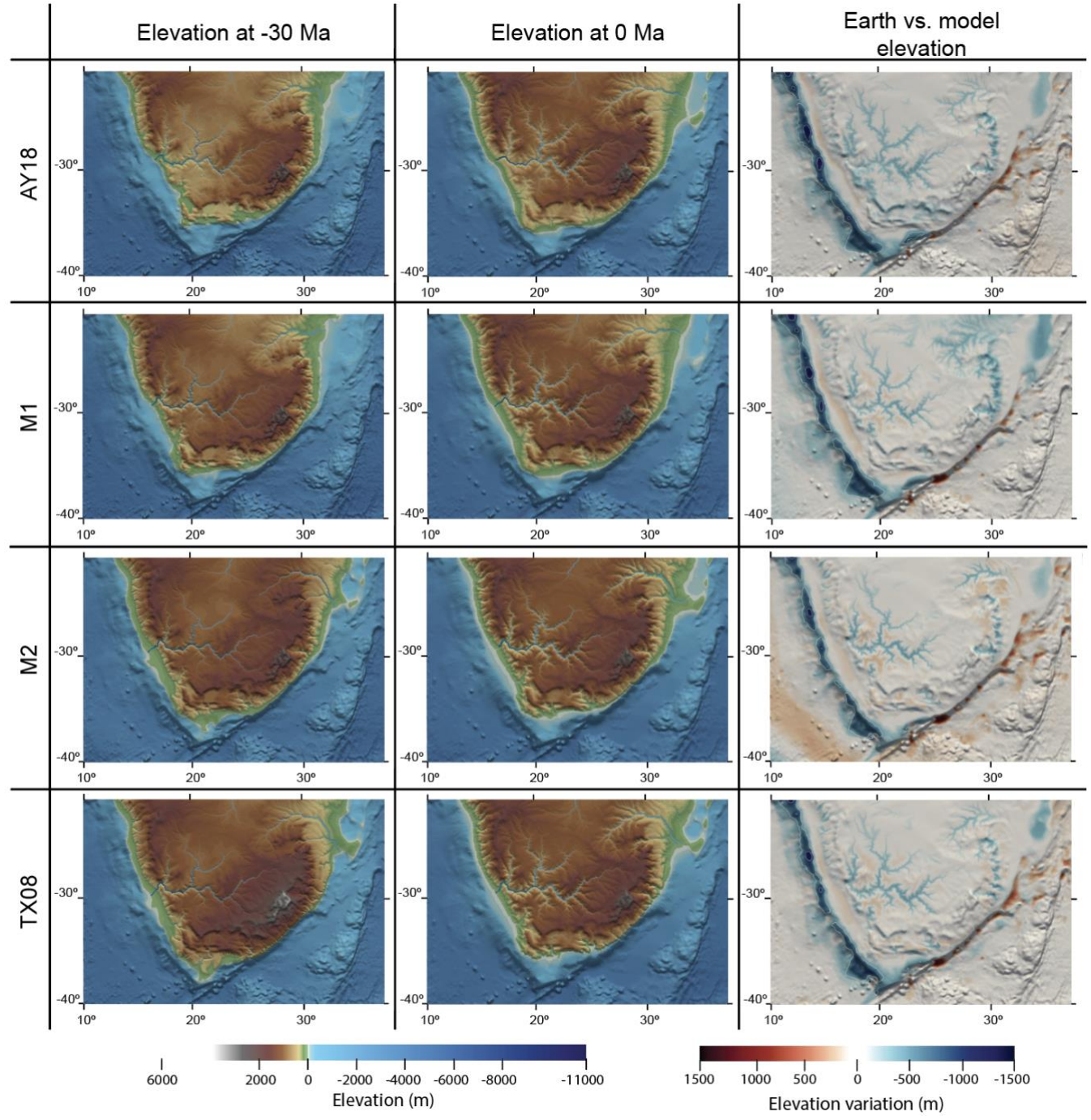

Figure 2: Surface evolution models. a. Reconstructed topography at 30 Ma resulting from the pseudo inversion method for the four mantle convection models. b. resulting topography at 0 Ma and c. differences between the actual Earth elevation and the elevation of the models at 0 Ma showing too low elevations of the models compared to Earth in blue and too high elevations in red.

https://doi.org/10.5194/esurf-2021-89
Preprint. Discussion started: 8 December 2021

3.2 Forward simulations

After inverting the dynamic topography impact, we use the four-resulting paleo-elevations to simulate the landscape evolution associated with each mantle driven uplift-subsidence scenarios using Badlands landscape evolution model (Salles et al., 2016; 2018; Appendix A). To insulate the dynamic signal from the climate forcing in the sedimentation record, we first test a first series of experiments with a uniform reference precipitation of 0.6 m/yr., approximating the present-day rate of precipitation in the Orange catchment basin. From produced initial paleo-elevations and based on the different forcing conditions presented above, we then run a series of landscape elevation models accounting for the flexural isostatic responses associated with plate loading and unloading induced by erosion and sedimentation (Wickert et al., 2016, Appendix A, Table A1). Our simulations do not include the effect of chemical weathering as well as rollover, mass loss which implies a bias on sediment thickness and sediment fluxes compared to data driven models (Rouby et al., 2009, Guillocheau et al., 2012, Dauteuil et al., 2013, Baby et al., 2020).

4 Sensitivity of the South African landscape to dynamic topography and climate variations

4.1 Topography

We first observe the contrasting initial topographies induced by the four tested scenarios. The models with the higher uplift rates (AY18 and M1; Figs. 1a and 2a) have the lowest initial elevation. The initial topography of M2 shows a homogeneous east-west topography induced by the heterogeneity of the east-west dynamic topography variations. M2 and TX08 show a regression of several kilometres on the western South African margin and TX08 shows a Lesotho massif culminating at 600 meters higher than its current elevation.

We run a first series of landscape evolution models with a fixed rainfall of 0.6 m/yr. The results show that after 30 Myr of evolution, the four simulated topographies are close to the present day (less than 100 m of variation in elevation within the Orange river catchment; Figs. 2b & c.), while the margins exhibit more differences induced by both sediment loading, isostatic adjustment (initial and temporal) and erodibility approximations bringing less material on the source area. The simulated location of the Orange River (and catchment; Fig. A4) are in accordance with its actual location but incisions are deeper than present day (up to 200 m of erosion). We attribute this mismatch to the initial surface elevation reconstruction approach that we used where sediments removed from the Orange sedimentary basin have not been redistributed across the catchment (Appendix A). Nevertheless, this underestimation does not bias our results as we focus on the variation of sediment fluxes through the last 30 Ma. To be specific and better quantify this bias, we compare the actual erosion rate of our models with cosmogenic radionuclide-based bedrock erosion rates. The final erosion rates predicted by our models range from 0.5 m/Ma for M1 (Fig. A5) to a maximum of 10 m/Ma for TX08. These values fit with published erosion rates inferior to 10 m/Ma (Cockburn et al., 2000, Kounov et al., 2007, Erlanger et al., 2012, Decker et al., 2013, Scharf et al., 2013, Dirks et al., 2016). It is worth mentioning that this comparison between models values vs. cosmogenic analyses can only be used as a first order estimation as it was performed in various erodible bedrocks.

https://doi.org/10.5194/esurf-2021-89
Preprint. Discussion started: 8 December 2021

Earth Surface Dynamics Discussions
Open Access
EGU

4.2 Sedimentary fluxes

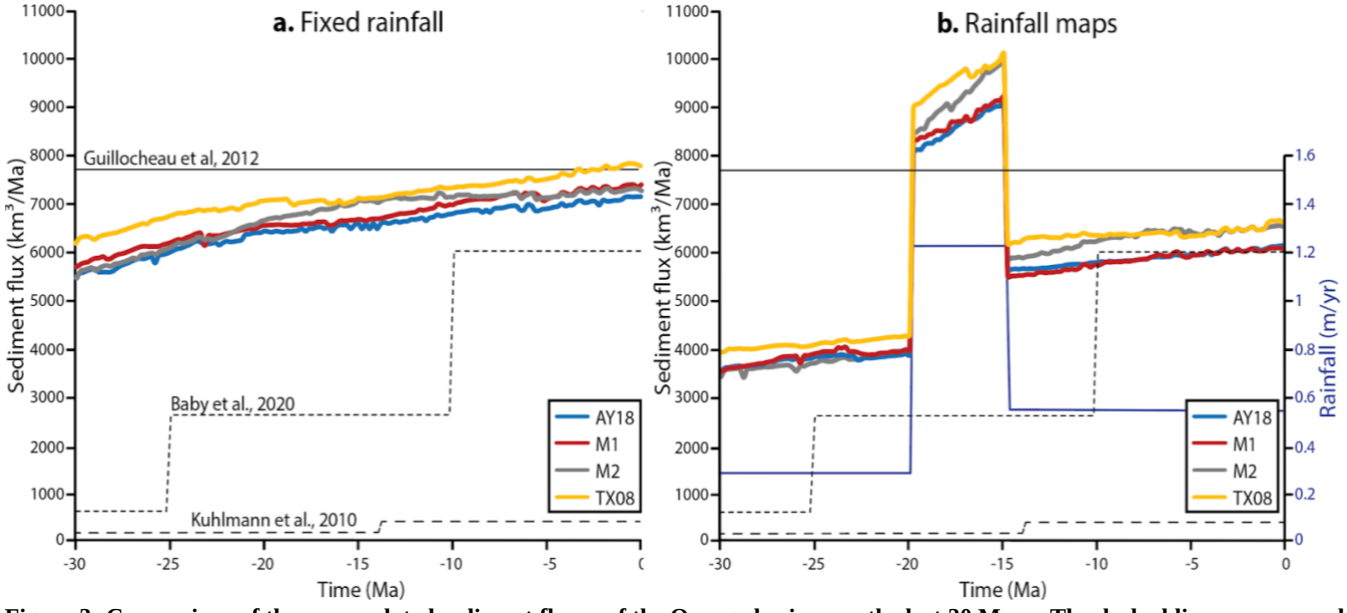

Figure 3: Comparison of the accumulated sediment fluxes of the Orange basin over the last 30 Ma. a. The dashed lines correspond to the fluxes calculated from the landscape evolution models with a fixed rainfall value at 0.6 m/yr. and b. The straight lines represent the fluxes of the models with spatial and temporal rainfall variations. The simulated fluxes extracted from the models with AY18 are in blue, M1 are in red, M2 are in grey and TX08 are in yellow. The estimated fluxes calculated from Earth data are in black.

When considering landscape evolution models with a fixed rainfall, the four sediment fluxes extracted at the Orange river mouth do not vary significantly through time (Fig. 3a, coloured lines). These values have the same magnitudes as the fluxes from Baby et al., 2020 but they do not fit with the increasing predicted fluxes over the Miocene, Eocene and Neogene. Our models, instead, capture finer but stable variations of sedimentary flux (every 100 000 years) around 5000 km^3/Ma. The simulated values are comparable with the stable post rift accumulation rate of Guillocheau et al., 2012 and Braun et al., 2014. The mismatch between both values, simulated and previously published from earth-modelled fluxes, can be attributed to the correction of carbonate proportion, volcanic production, porosity removal and chemical weathering (Guillocheau 2012, Rouby et al., 2012). For example, the estimated volume of sediments for the Orange basin in Rouby et al., 2012 is doubled assuming that half of the volume of sediment removed has been lost to chemical weathering (Larsen et al., 2014). Simulated fluxes for the different dynamic topography histories have similar trends. As this first series of tests considers fixed rainfall, this suggests that none of the tested dynamic topography models are able to drive the large pulse of erosion observed across the South African plateau over the last 25 Ma (Baby et al., 2020).

To evaluate the combined effects of dynamic topography estimations and precipitation on sediment flux delivered to the Orange river mouth, we run four additional simulations forced with variable rainfall conditions (Appendix A, Fig. A1). The precipitation maps used to force the model imply drastic sedimentary flux changes (Fig. 3). Adding variable rainfall maps

https://doi.org/10.5194/esurf-2021-89
Preprint. Discussion started: 8 December 2021

induce an average rainfall increase in the Orange catchment basin by a factor of 4.4 (from 0,26 to 1.24 m/yr.; Fig. 3) between 20 and 15 Ma whilst the sedimentary flux increases in the same period by a factor of 2.2 in average.

The sediment fluxes extracted from the four models incorporating dynamic topography and climate variations follow the imposed climatic variations with highest values during the most humid period (between 8000 km^3/Myr and 10000 km^3/Myrs, Fig. 3b, coloured straight lines). Despite the impact of both dynamic topography and climate variations, the size of the Orange River catchment does not significantly change through space and time (Fig. A4). This indicates that if the Orange basin sedimentary flux is extremely sensitive to climate variations, these changes associated with dynamic topography variations do not influence the erosion enough to reshape the landscape and reorganise the drainage system. We see that the proposed variation of rainfall between 30 and 15 Ma can produce a similar amplitude of sedimentary flux variation as in Baby et al., 2018 (Fig. 3b). Nevertheless, this increase is contained between 20 and 15 Ma in our case (based on the climate maps that we derived from available paleo-dataste) and does not have a constant increasing pattern. This can be explained as the climate is more humid on the eastern margin over the last 15 million years but overall drier on the western margin where the imposed erodibility is higher.

4.3 Correlations between erosion, climate, and dynamic topography

To quantitatively analyse the importance of each forcing mechanism, we extract different Spearman correlation indices (Appendix A) to measure the degree of association between 1) the instantaneous erosion, 2) the dynamic topography impact and 3) climate in the Orange river catchment (Fig. 4).

We test correlation between erosion and the average of dynamic topography as well as dynamic topography at specific altitudes (850m, between 850 and 1350m and above 1350m; Fig. A5) under uniform and spatially variable precipitation rates. These specific altitudes have been chosen as the uplift associated with dynamic topography can vary between the western and the eastern part of South Africa (Fig. 1) but also because they correspond to different erodibility provinces; for example, Karoo basin contains sandstones intruded by dolerites which are more subject to erosion than the high overlapping basalts of Lesotho. Even if we look at the correlation between instantaneous erosion and dynamic topography in the catchment, the simulated erosion in our simulations is always the product of three components: uplift, erodibility and rainfall.

https://doi.org/10.5194/esurf-2021-89
Preprint. Discussion started: 8 December 2021

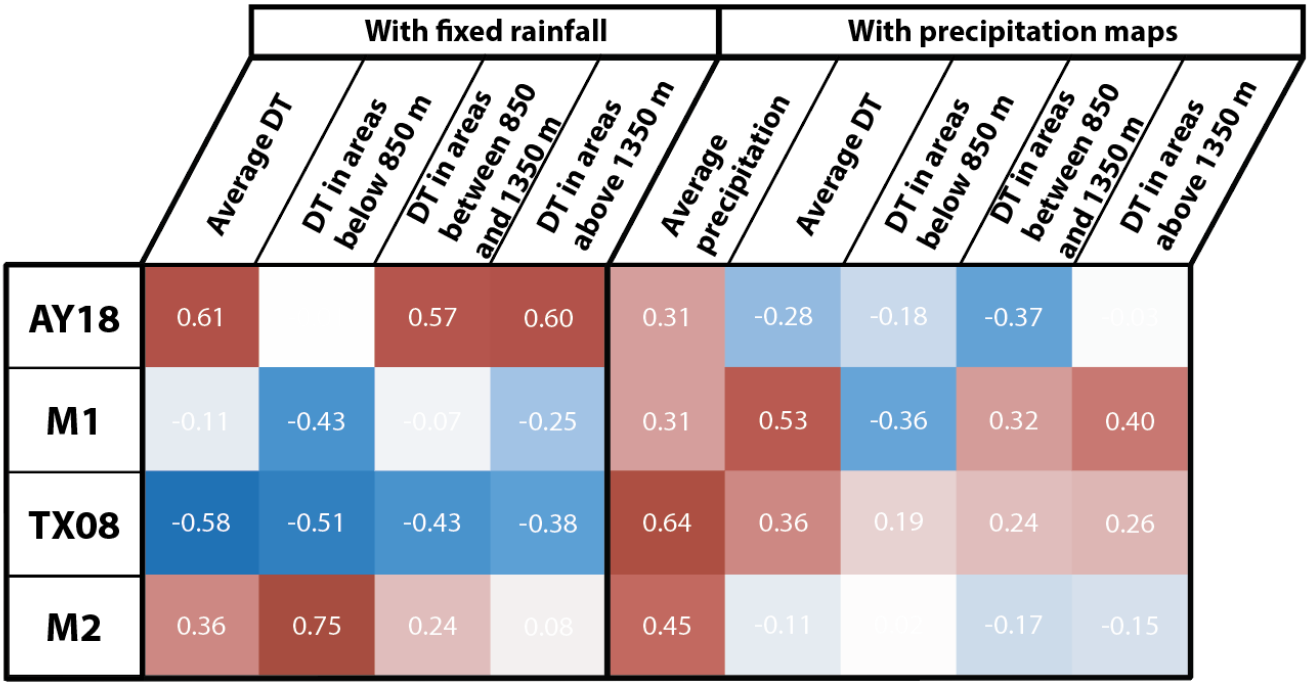

Figure 4: Correlation heatmap. Correlations between the instantaneous erosion with the average dynamic topography (DT), the DT in the areas below 850m, the dt in the areas between 850 and 1350 m, the areas above 1350 m as well as the average precipitation changes in the Orange catchment basin. These correlations are calculated under a uniform precipitation rate of 0.6 m/yr. and spatial precipitation variations for the four tested dynamic topography scenarios. High correlations are in red, high anticorrelations are in blue. Correlations values superior to 0.70 indicate a very strong positive relationship, between 0.69 and 0,40 a strong positive relationship, between 0.39 and 0.30 a moderate positive relationship, between 0.29 and 0.20 a weak positive relationship, between 0.19 and 0.01 no or negligible relationship and 0, no correlation.

For the model AY18, when precipitation is uniform, there is a strong positive correlation between the uplifted areas above 850m (Fig. 4: 0.57 and 0.60) and the instantaneous erosion of the catchment. This model contains the most important dynamic topography uplift, especially around the Lesotho (Fig. 1). In contrast, when the climate variation is turned on, the correlation between erosion and dynamic topography (Fig. 4: -0.28) is anticorrelated and non-significant compared to the moderate positive relationship between climate and erosion.

The model M1 results in a small uplift, around 50 meters over the last 30 Ma, of the eastern part of the catchment (Fig. 1) which did not act on the erosion of the catchment whilst an anticorrelation between uplift and erosion is strongly positive on the subsiding western part of the catchment (Fig. 1; Fig. 4). When the precipitation maps are turned on, the eastern and most elevated parts of the plateau, which experienced the most humid conditions between 0 and 15 Ma, highlight a stronger relationship between uplift and erosion (0.32 and 0.40: strong and moderate positive correlations).

The model TX08 experienced the highest subsidence rate of all tested dynamic topography scenarios. We see that for this model, the anticorrelation rates between uplift and erosion are highest, strongly positive anticorrelations for the area below

https://doi.org/10.5194/esurf-2021-89
Preprint. Discussion started: 8 December 2021

1350m, and moderate positive for the highest areas (Fig. 4). When we add temporal and spatial precipitation to this model, we can see that average climate and erosion are strongly correlated (0.64, Fig. 4).

In the last M2 scenario, we observe a very strong correlation between the erosion in the lowest area of the catchment and the imposed subsidence. Nevertheless, when the spatial and temporal precipitation variations are added into the model, this positive correlation between uplift and erosion is replaced by a strong positive correlation between climate and instantaneous erosion in the Orange river catchment.

Here we observed that dynamic topography impact in the models AY18, TX08 and M2 is smoothed by the impact of spatial and temporal precipitation variations. The dynamic topography influenced on the South African erosion also appears to be non-significant for model M1, especially for the areas above 850 m. Here, not only the imposed uplift/subsidence associated with dynamic topography vary between the eastern and western part of the Orange catchment but also does the climate condition, the erodibility as well as the slopes of the initial and evolving landscape. All these parameters have an impact on the instantaneous erosion which differs depending on their prevalence through time. For example, if the erodibility variation is fixed for the model TX08, then the correlation between erosion and uplift decreases in the highest area and increases in the area below 1350m (Fig. A7).

4.4 Depocenters locations

We saw that climate is a major driver of sedimentary fluxes on the Orange Basin for the model M2, TX08 and AY18, especially when the eastern and western part of the Orange catchment have the same uplift history (Model AY18). In Fig. 5, we see that depending on the uplift forcing, the location and the thickness of deposits change. Increased marine accumulations are observed when considering models M2 and TX08. Models AY18 and TX08 contain less deposited sediments in the southern basins than models M1 and M2. Only models AY18 and TX08 show a preferential accumulation of sediments in accordance with actual observations, i.e., close to the Orange river mouth (Rouby et al., 2012, Braun, 2014).

https://doi.org/10.5194/esurf-2021-89
Preprint. Discussion started: 8 December 2021

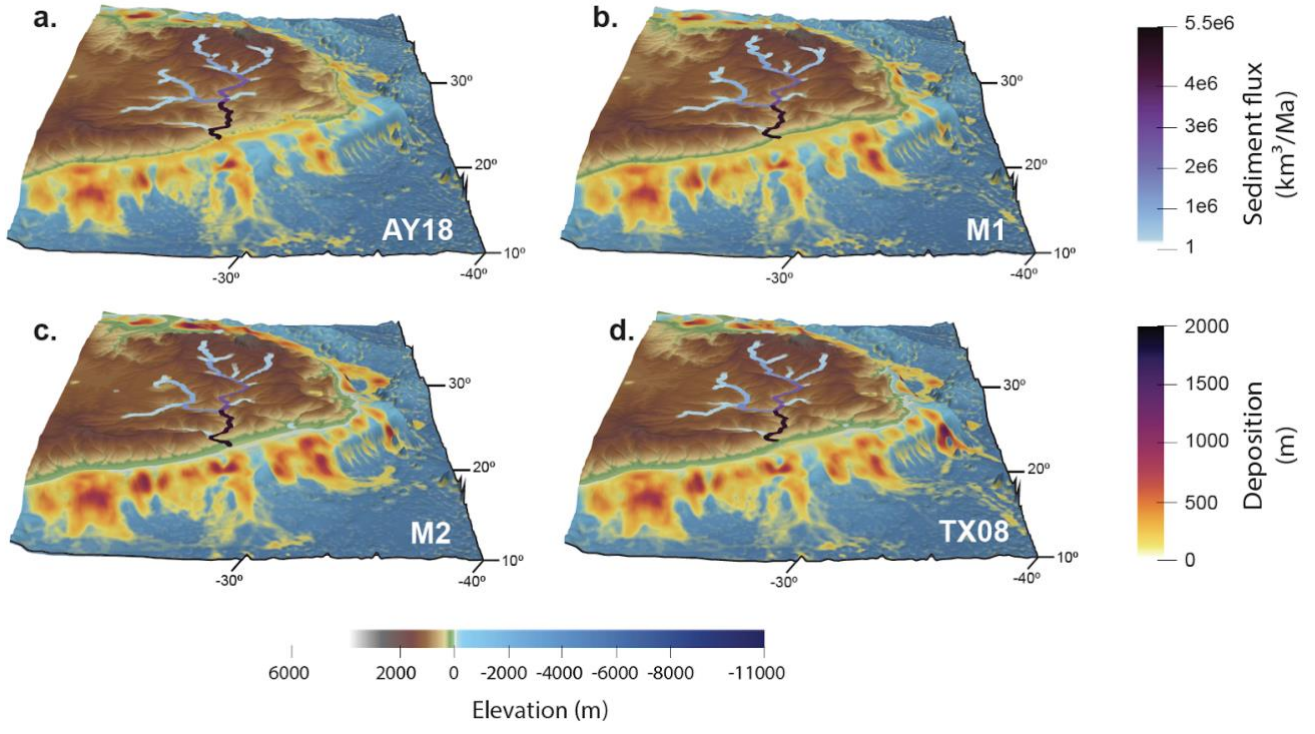

Figure 5: Modelled surface elevations for the four tested dynamic topography scenarios with uniform precipitation. The main depocenters with accumulations superior to 500 are in orange to purple. The drainage of the Orange river is highlighted with spatially variable sediment fluxes from light blue: smallest sediment fluxes to black: highest sediment fluxes.

5 Conclusions

Here we explored different scenarios of South African mantle uplift differing by their amplitudes and timings. We inverted mantle-driven forces to obtain the paleo-elevation of South Africa 30 Myrs ago. None of the tested dynamic topography scenarios allow to generate the same variations of sediment flux as data-based estimations. We recognise that this might be due to an underestimation of the uplift associated with dynamic topography calculations (removal of the first 250 km of upper mantle for example). We actually found that after doubling the dynamic topography estimation (Fig. A6), we could observe a strongest correlation between dynamic topography and erosion of the Orange river catchment.

Here we demonstrate that if rainfall variations through space and time can generate the same pulse amplitude as sediment flux observed in the Miocene (Baby et al., 2018; 2020), our actual knowledge of the South African climate cannot predict the entire increasing pattern. Incorporating climate variations in landscape evolution models showed how climate smoothed the dynamic topography impact, especially if in scenarios where differential uplift also affected the eastern and western margin of South Africa (model TX08 for example). We show the importance of taking climate, dynamic topography as well as erodibility together as forcing parameters and not only focusing on one main driver as they appear to be completely interdependent.

https://doi.org/10.5194/esurf-2021-89
Preprint. Discussion started: 8 December 2021


Earth Surface Dynamics Discussions
Open Access
EGU

We agree that mantle dynamics can cause rapid uplift associated with drainage reorganisation, and denudation over a short period of time (Ding et al., 2019). Braun et al. 2013, also showed that low slopes associated with the motion of a continent over a fixed source of dynamic topography may lead to substantial, i.e., kilometre scale, and rapid surface erosion, through continental-scale drainage reorganization. Erosion is linked with dynamic topography scenarios in this study, however, none of them can generate an increase of sedimentary fluxes compatible with Baby et al., 2018. Our results suggest that sediment accumulation in the shelf might have happened as a consequence of an earlier plume impact (Gurnis et al., 2000) that might have induced a more significant uplift.

If the remaining mantle flow is not able to generate major changes in the source-to-sink system of the Orange River catchment over the last 30 Myrs, it strongly influences the location of depocenters in the Orange basin. This paper includes new modelled sedimentary flux data which allows us to understand the uplift history of South Africa as well as the climate impact over the last 30 Ma. The method used here is a first step to reconcile Earth data and landscape evolution models and proposes a new framework to fill the data gap for the South African surface evolution. This work opens new perspectives to understand the interplay between tectonic, mantle, and surface processes in the context of climate, erodibility and sea level change, not only in South Africa but all around the margin basins.

Appendix A:

Pseudo inversion method to generate the initial topography. The initial paleo elevations have been generated by removing the dynamic topography impact as well as the load of sediments and associated flexural component (Fig. A3, Table A1) from the global digital elevation model of present-day Earth ETOPO1 at 1 arc-minute resolution (NOAA, 2021) following the method:

$$T_{30} = T_0 - (\sum_{t=5} \Delta \mathrm{dt}) - S_{30} + D_{30} \quad (1)$$

where T_{30} is the initial paleo-topography (m), T_0 is the actual topography (m), dt is the uplift value associated with the geodynamic models, t is the timesteps between dynamic topography timesteps (yr.), S is the sediment thickness for the last 30 Ma (m) and D is the deflexion (m) induced by the load of sediments removal. We compiled existing sediment thickness maps (Seranne and Anka 2006, Rouby et al., 2009, Kuhlmann et al., 2010, Maystrenko et al., 2013, Baby et al., 2018) as well as cross-sections along the Orange basin (De Vera et al., 2010, Guillocheau et al., 2012, Dauteuil et al., 2013, Baby et al., 2020) to produce a sediment thickness map for the last 30 Ma (Fig. A3). The flexural parameters used to calculate the deflexion induced by the removal of these sediments are synthesized in the Fig. A3 and Table A1. To take the effect of the load or removal of sediments into account on the initial deflection and flexural isostasy through time, we used the python module gFlex with finite difference approximation as we used non-uniform lithospheric elastic thickness values (Wickert, 2016).

https://doi.org/10.5194/esurf-2021-89
Preprint. Discussion started: 8 December 2021

Landscape evolution models. The surface evolution models have been generated using the open-source code Badlands (Salles, 2016, Salles and Hardiman 2016, Salles et al., 2018) which allows to simulate surface processes including fluvial, hillslope, and wave-induced sediment transport, as well as the growth of coral reefs (Salles et al., 2018). The governing equations of the simulated processes and detailed documentation are available on https://badlands.readthedocs.io and input scripts here: https://github.com/clairemallard/SouthAfricanLandscape_30Ma .

The default detachment-limited stream power law is used to account for river incision and hillslope processes using a soil creep linear diffusion equation where 3 diffusions are defined: 15 m^2/yr. for river-transported sediments, 1.5 m^2/yr. for the subaerial realm and 0.5 m2/yr. for the marine realm. Below the base level, sedimentation occurs within enclosed basins or offshore areas, or when local slope is below 0.01. Coastal deposition is defined by the steps used to distribute marine deposit (diffnb = 5) and the diffprop parameters set to 0.01 which translate the maximum thickness that can be deposited on downstream nodes accounting for dispersal of sediment into marine environments.

Erodibility. The South African craton is defined by strong erodibility contrasts between its different lithologies, i.e., the metamorphic and magmatic rocks, the siliciclastic sequence of the Karoo basin and mafic rocks (Catuneanu et al., 1998). Braun et al., 2014 demonstrated that the volume of soft sediments can strongly influence the sedimentation of South Africa. We included spatially variable lithologies through the implementation of an erodibility map (Fig. A2) generated via an erodibility index (Moosdorf et al., 2018, Table A2) which is based on the South African lithologies.

Flexure. As detailed above, we account for flexural isostasy responses induced by the erosion and deposition via the python package gFlex (Wickert, 2016) included in Badlands. The detailed parameters are available in Table A1 and the lithospheric elastic thickness used is presented in Fig. A3 (Perez-Gussinye et al., 2009).

Climate variations. Here we present three paleoclimate maps (Fig. A1) based on the compilation of paleo-precipitation indicators including vegetation assemblage (Bamford 2000), dated foraminifera, pollens, and mammals (Tyson and Partridge, 2000, Braun et al., 2014). At the end of the Eocene (33 Ma), Salman and Abdula 1995, propose a major climate change due to a glacial event occurring during the Oligocene and lowermost Miocene (34-20 Ma), therefore there is a lack of data during this period. Here we base our climate map (Fig. A1a) on Macgregor 2010; 2013 studies, which describe a tropical to semi-arid and arid climate from middle Africa to the south of South Africa. We created the Figure A1b following the same studies. Nevertheless, we recognise that Dauteuil et al., 2015 interpret the presence of kaolinite and saprolite as markers of a weathering profile in South Africa from 27.4 Ma to 5.2 Ma and other authors agree on a more humid coastal climate during the Burdigalian (20-16 Ma) (Pickford and Senut, 1999; Braun 2014, Salman & Abdula 1995), with pluvial stage in the actual Namid desert (Bamford and Dewitt 2013). To integrate these data, we extended a sub humid area on the south of South Africa (Fig. A1b). As authors consider more arid events (with a relatively humid plateau) around 15 Ma (Pickford and Senut, 1999; Ségalen et al., 2006, Braun et al 2014, Salman and Abdula 1995), we used the actual rainfall range from 15 to 0 Ma (Burke and Gunnell

https://doi.org/10.5194/esurf-2021-89
Preprint. Discussion started: 8 December 2021

2008). This incorporates the conclusion of Senut and Pickford that the climate was more arid in the Neogene (23-3Ma). Even if some authors argue that there is a short wetter period during the Plio-Pleistocene (after 5.3Ma, Ward and Corbett 1990, Bamford and 2013), it is difficult to constrain this event and we consider that the arid climate is still active (Fig. A1c).

Correlation methods. The heat maps presented in this study compiled robust statistical cross-correlation coefficients between instantaneous erosion and the rainfall or dynamic topography variations. We used the Spearman rank correlation to measure the degree of association between these variables as it does not require any assumptions on data distribution. It is usually a more robust and stable estimate than the Pearson analysis.

Model limitations. Some of these limitations are intrinsic to all numerical landscape evolution models. For example, the nature of simulated sediments is temporally and spatially uniform (Salles and Hardiman, 2016). Another limitation is the spatial and temporal resolution of the models (5 km and 200,000 yrs. time steps), which prevent the integration of local and short-term features as small catchments and river reorganisations for example. The time steps also imply non-realistic and drastic changes in the sedimentary fluxes variations (Fig. 3). The diffusion and slopes coefficient are another approximation impacting the sedimentation and the landscape elevation. These types of imposed parameters are not directly supported by data. For example, the spatially variable erodibility values as well as the fixed ones (Fig. A7) are not constrained by data but by an erodibility index (Table A2) and a series of models to match both present-day elevation and sediment distribution of South Africa. Another reason these models must be tempered is that the material removed from the margin in the backward step is not added back in the Orange catchment basin before the forward step. Therefore, the analysis presented here focused on sediment fluxes, relative differences in sediment volumes between models and not absolute sediment volumes. Other imposed data come from interpretations or models where the uncertainties are not quantified such as the dynamic topography estimations. The uplift rates or sedimentary fluxes used as "earth data" themselves are inferred from apatite fission track, thermochronometric data exhumation rates, seismic reflections, introducing another level of uncertainty.

Another limitation is that the sea-level curve used (Hacq 1987) has a temporal resolution finer than the timestep resolution of the models, yet the coastal sedimentation is also biased. The impact of longshore drift or bottom current like the Aguilas one is not considered while it is essential to obtain a more accurate sedimentation prediction on the eastern and southern margin of South Africa. These limitations do not affect the results of our study as we focused on the evolution of the western margin. The paleo precipitation maps were constrained by the limited availability of data resulting in a patchwork of data (Appendix A; Climate) and do not account for altitude variation. Their level of accuracy cannot be quantified whilst precipitation is one of the major controls on erosion rates. Even if the uncertainties involved in the creation of such the paleo precipitation maps may have contributed to differences between data and model results, here we do not focus on values but on the impact of rainfall variations on erosion and sedimentation.

https://doi.org/10.5194/esurf-2021-89
Preprint. Discussion started: 8 December 2021

Earth Surface Dynamics Discussions
Open Access
EGU

360 - **Appendix A figures**

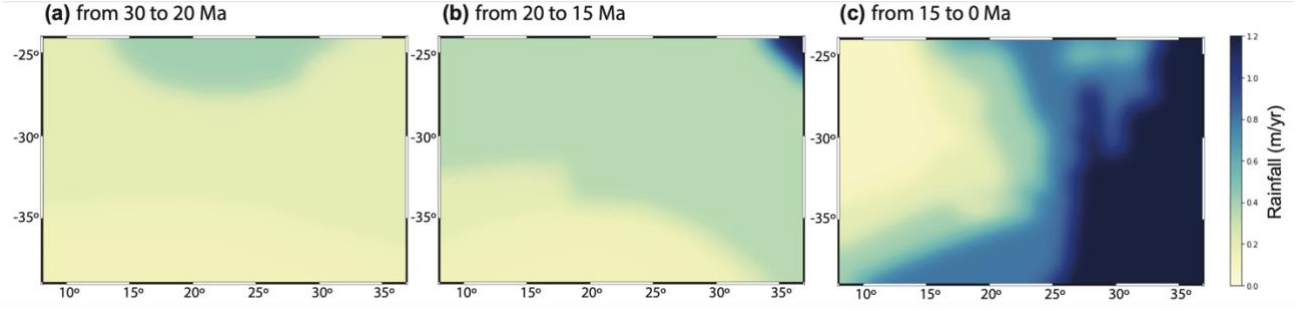

Figure A1: Rainfall maps used to constrain the surface evolution models. The black line represents the actual coastline of South Africa of the model M1.

365

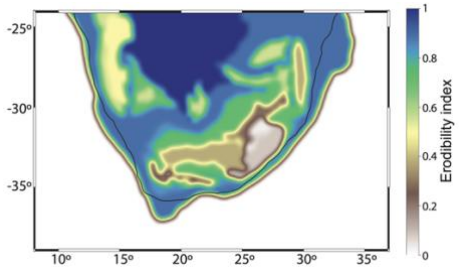

Figure A2: Erodibility map accounting for lithological variations obtained using Supplementary Data Table 2. The black line represents the actual coastline of South Africa of the model M1.

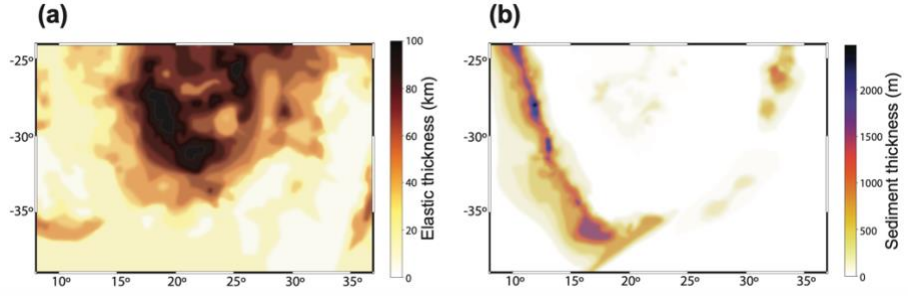

370 **Figure A3: Flexure calibration maps. a. lithospheric elastic thickness map modified from Perez-Gussinye et al., 2009. b. Sediment thickness map estimated with Intawong et al., 2019, Baby et al., 2018, Koopman et al, 2014, Dauteuil et al., 2013, Maystrenko et al., 2013, Guillocheau et al., 2012, Kuhlman et al., 2010, Rouby et al., 2009. The black line represents the actual coastline of South Africa of the model M1.**

375

https://doi.org/10.5194/esurf-2021-89
Preprint. Discussion started: 8 December 2021

Earth Surface Dynamics Discussions
Open Access
EGU

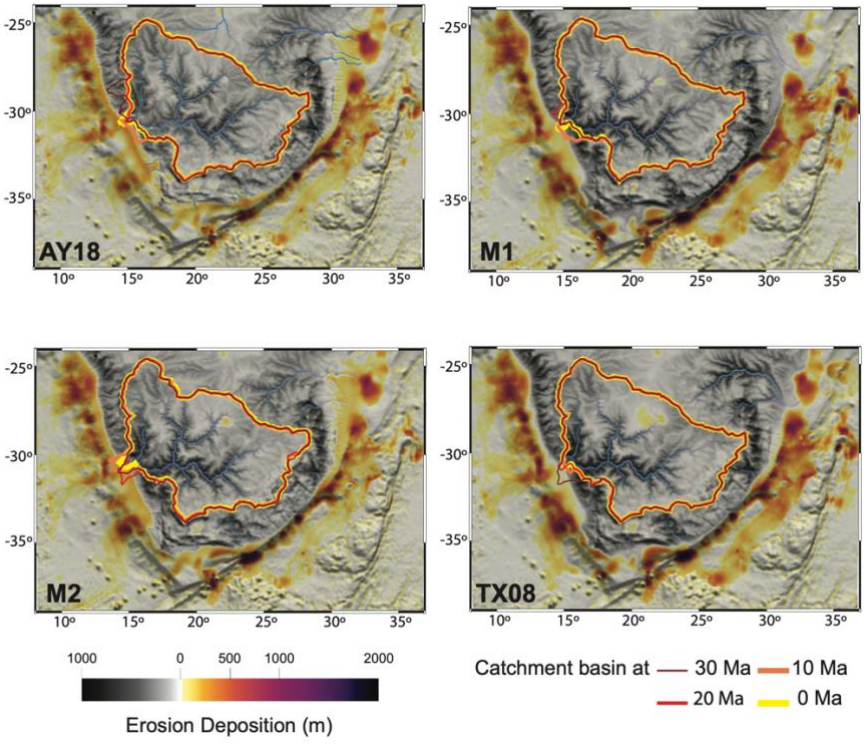

Figure A4: Erosion maps of the Orange source to sink systems. Erosion deposition maps after 30 Myrs of evolution for the four dynamic topography estimations. The location of the Orange river catchment is surrendered in dark red at 30 Ma, red at 20 Ma, orange at 20 Ma and yellow for the present day location.

380

https://doi.org/10.5194/esurf-2021-89
Preprint. Discussion started: 8 December 2021

Earth Surface Dynamics Discussions
Open Access
EGU

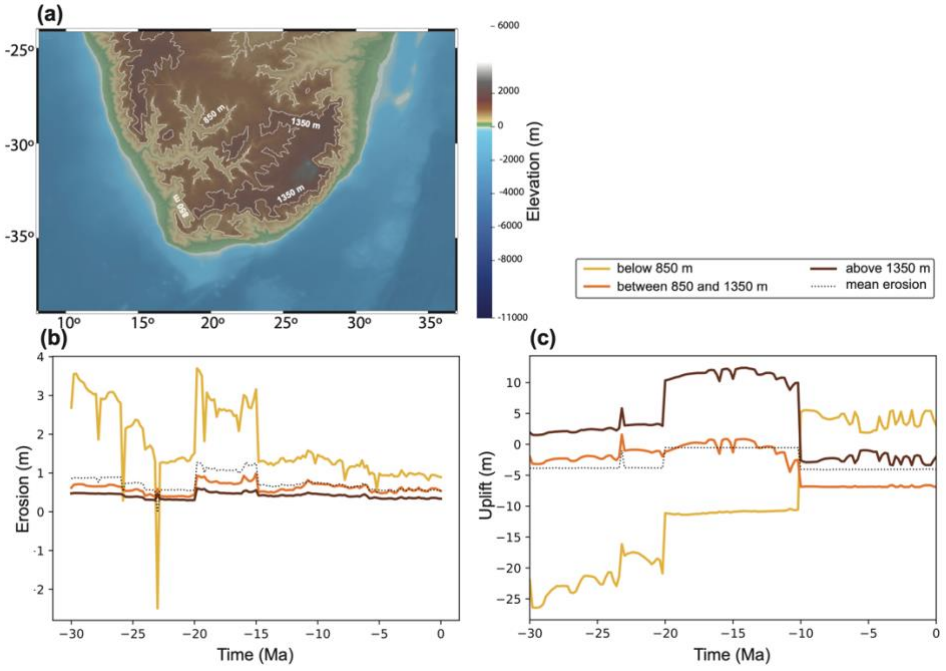

Figure A5: Erosion domains considered to calculate the correlation between instantaneous erosion, climate, and dynamic topography for the model M1. a. Shows the different domains. b. Erosion graphs depending on three domains: below 850m in yellow, between 850 and 1350m in orange and above 1350 in brown. Mean erosion values are represented by the black dashed line. c. Uplift variations for the scenario M1 depending on the same three domains. The mean uplift values are represented by the black dashed line.

	Average precipitation	Average DT	DT in areas below 850 m	DT in areas between 850 and 1350 m	DT in areas above 1350 m
Rainfall uniform at 0.6 m/yr DT * 1	Na	-0.11	-0.43	-0.07	-0.25
Precipitation map DT * 1	0.31	0.53	-0.36	0.32	0.40
Rainfall uniform at 0.6 m/yr DT * 2	Na	0.29	-0.62	0.23	0.13
Precipitation map DT * 2	0.45	0.63	-0.19	0.50	0.54

Figure A6: Heatmap representing the correlation between instantaneous erosion, uplift, and rainfall for the simulation M1 and for a simulation with increasing dynamic topography by a factor two. High correlations are in red, high anticorrelations are in blue.

https://doi.org/10.5194/esurf-2021-89
Preprint. Discussion started: 8 December 2021

Earth Surface Dynamics Discussions
Open Access
EGU

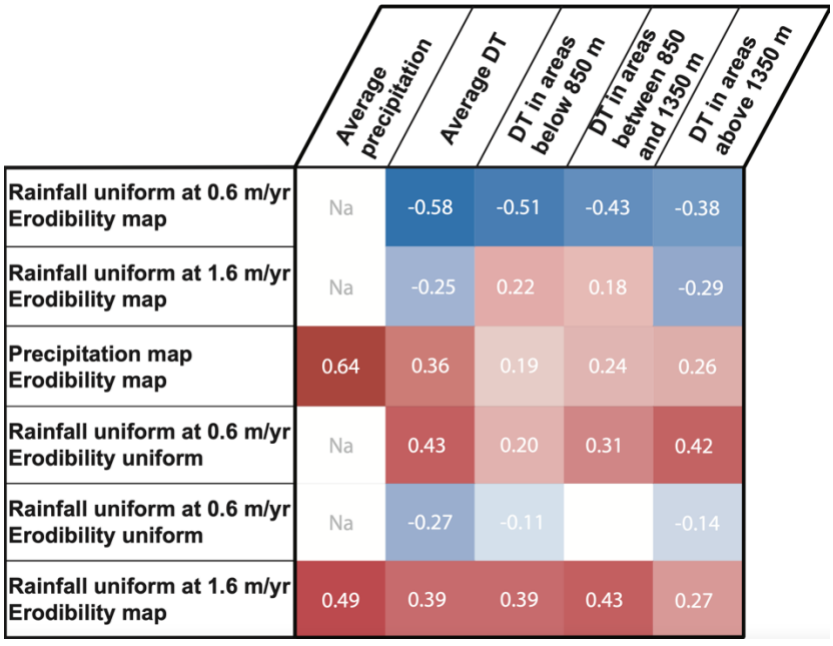

Figure A7: Heatmap representing the correlation between instantaneous erosion, uplift, and rainfall for the model TX08 with variable or fixed climate and erodibility. High correlations are in red, high anticorrelations are in blue.

395

- **Appendix A tables**

Grid Setup	Resolution	5 km
	Time interval	200000 yrs
	Sea Level	Hybrid curve from Hacq et al., 1987
Precipitation	Fixed	0.7 m/yr
	Changing	Precipitation maps see figure A1
Erodability	Fixed	1.6 e-7
	Changing	Erodability maps see figure A2
Flexure	Mantle density	3340 kg/m3
	Sediment density	2670 kg/m3
	Young's Modulus	100e9 Pa
	Lithospheric elastic thickness	Map see figure A3
Dynamic topography estimations	M1	Combined backward/forward convection model from Gurnis et al. 2012, Muller et al., 2018
	M2	Mantle convection model from Hassan et al., 2020 with tectonic reconstructions modified from Seton et al. 2012
	AY18	Mantle convection model from Cao et al., 2019 with global plate tectonic reconstructions of Young et al. 2018
	TX08	Model derived through a joint inversion of global seismic & geodynamic data sets from Moucha and Forte 2011

400 **Table A1: Badlands parameters datasets. Grid and flexure parameters and tested rainfall and dynamic topography scenarios used to force landscape evolution models**

https://doi.org/10.5194/esurf-2021-89
Preprint. Discussion started: 8 December 2021

Erodibility index	Lithology
1.0	Acid plutonic rocks, metamorphic rocks, and carbonate sedimentary rocks
1.1	Acid volcanic rocks
1.2	Mixed sedimentary rocks
1.4	Basic volcanic rocks
1.5	Basic plutonic rocks, siliciclastic rocks of all grain sizes
3.2	Unconsolidated sediments

Table A2: Erodibility index accounting for the different lithological classes from Moosdorf et al., 2018.

Code availability

The Badlands code is open source and available via Docker. All documentation is available here: https://badlands.readthedocs.io/en/latest/index.html
Scripts availability: https://github.com/clairemallard/SouthAfricanLandscape_30Ma

Data availability

Inputs availability: the lithology map used to create the erodibility map is available here: https://maps.geoscience.org.za/portal/apps/webappviewer/index.html?id=f17eb56408b34add9c43878de5ccd4c2
Availability of the models AY18, M1 and M2: http://portal.gplates.org/portal/dt/

Author contribution

C.M. and T.S. developed the scientific concepts presented herein, conducted the experiments, analysed the results, and wrote the paper.

Competing interests:

The authors declare that they have no conflict of interest.

Acknowledgements

The research leading to this manuscript was supported by the ARC grant IH130200012 and the project STELLAR. The mantle convection models have been generated thanks to the assistance of resources from the National Computational Infrastructure (NCI), which is supported by the Australian Government.

https://doi.org/10.5194/esurf-2021-89
Preprint. Discussion started: 8 December 2021

References

Baby, G., Guillocheau, F., Boulogne, C., Robin, C., and Dall'Asta, M.: Uplift history of a transform continental margin revealed by the stratigraphic record: The case of the Agulhas transform margin along the Southern African Plateau. Tectonophysics, 731–732, 104–130, https://doi.org/10/gg6wn2, 2018.

Baby, G., Guillocheau, F., Braun, J., Robin, C., and Dall'Asta, M.: Solid sedimentation rates history of the Southern African continental margins: Implications for the uplift history of the South African Plateau, Terra Nova, 32(1), 53–65. https://doi.org/10/ggw55p, 2020.

Bamford, M. K., Partridge, T. C. and Maud, R. R., Cenozoic macro-plants, in The Cenozoic of Southern Africa, Oxford Monographs on Geology and Geophysics, 40, 351-35, 2000.

Braun, J., Guillocheau, F., Robin, C., Baby, G., and Jelsma, H.: Rapid erosion of the Southern African Plateau as it climbs over a mantle superswell, Journal of Geophysical Research: Solid Earth, 119(7), 6093–6112. https://doi.org/10/ggfrck, 2014.

Brown, R. W., D. J. Rust, M. A. Summerfield, A. J. W. Gleadow, and De Wit, M. C.: An Early Cretaceous phase of accelerated erosion on the southwestern margin of Africa: Evidence from apatite fission track analysis and the offshore sedimentary record, International Journal of Radiation Applications and Instrumentation. Part D. Nuclear Tracks and Radiation Measurements, 17(3), 339-350, 1990.

Brown, R. W., Summerfield, M. A., and Gleadow, A. J. W.: Denudational history along a transect across the Drakensberg Escarpment of southern Africa derived from apatite fission track thermochronology. Journal of Geophysical Research: Solid Earth, 107(B12), 2350, https://doi.org/10.1029/2001J B000745, 2002.

Burke, K.: The african plate. South African Journal of Geology, 99(4), 341–409, 1996.

Burke, K., and Gunnell, Y.: The African erosion surface: a continental-scale synthesis of geomorphology, tectonics, and environmental change over the past 180 million years, Geological Society of America, 201, 2008.

Cao, W., Flament, N., Zahirovic, S., Williams, S., and Müller, R. D.: The interplay of dynamic topography and eustasy on continental flooding in the late Palaeozoic, Tectonophysics, 761, 108-121, 2019.

Cockburn, H. A. P., Brown, R. W., Summerfield, M. A., and Seidl, M. A.: Quantifying passive margin denudation and landscape development using a combined fission-track thermochronology and cosmogenic isotope analysis approach, Earth and Planetary Science Letters, 179(3), 429–435, https://doi.org/10/dmssc4, 2000.

Dauteuil, O., Bessin, P., and Guillocheau, F.: Topographic growth around the Orange River valley, southern Africa: A Cenozoic record of crustal deformation and climatic change, Geomorphology, 233, 5–19, https://doi.org/10/gg6w26, 2015.

Dauteuil, O., Deschamps, F., Bourgeois, O., Mocquet, A. and Guillocheau, F.: Post break-up evolution and palaeotopography of the North Namibian Margin during the Meso-Cenozoic, Tectonophysics, 589, 103-115, 2013.

Decker, J. E., Niedermann, S., and de Wit, M. J.: Climatically influenced denudation rates of the southern African plateau: Clues to solving a geomorphic paradox, Geomorphology, 190, 48–60, https://doi.org/10/f4wwbs, 2013.

Ding, X., Salles, T., Flament, N., Mallard, C., and Rey, P. F.: Drainage and sedimentary responses to dynamic topography, Geophysical Research Letters, 46(24), 14385-14394, 2019.

Dirks, P. H. G. M., Placzek, C. J., Fink, D., Dosseto, A., and Roberts, E.: Using 10Be cosmogenic isotopes to estimate erosion rates and landscape changes during the Plio-Pleistocene in the Cradle of Humankind, South Africa, Journal of Human Evolution, 96, 19–34, https://doi.org/10/f8trm3, 2016.

Erlanger, E. D., Granger, D. E., and Gibbon, R. J.: Rock uplift rates in South Africa from isochron burial dating of fluvial and marine terraces, Geology, 40(11), 1019–1022, 2012.

Flowers, R. M., and Schoene, B.: (U-Th)/He thermochronometry constraints on unroofing of the eastern Kaapvaal craton and significance for uplift of the southern African Plateau, Geology, 38(9), 827–830, https://doi.org/10/bptpcp, 2010.

Forte, A. M., Quéré, S., Moucha, R., Simmons, N. A., Grand, S. P., Mitrovica, J. X., and Rowley, D. B.: Joint seismic–geodynamic-mineral physical modelling of African geodynamics: A reconciliation of deep-mantle convection with surface geophysical constraints, Earth and Planetary Science Letters, 295(3-4), 329-341, 2010.

Gilchrist, A. R., Kooi, H., and Beaumont, C.: Post-Gondwana geomorphic evolution of southwestern Africa: Implications for the controls on landscape development from observations and numerical experiments, Journal of Geophysical Research: Solid Earth, 99(B6), 12211–12228, https://doi.org/10/cknczm, 1994.

Green, P. F., Duddy, I. R., Japsen, P., Bonow, J. M., and Malan, J. A.: Post-breakup burial and exhumation of the southern margin of Africa, Basin Research, 29(1), 96–127, https://doi.org/10/f9r64k, 2017.

Guillocheau, F., Rouby, D., Robin, C., Helm, C., Rolland, N., De Veslud, C. L. C., and Braun, J.: Quantification and causes of the terrigeneous sediment budget at the scale of a continental margin: a new method applied to the Namibia-South Africa margin, Basin Research, 24(1), 3–30, https://doi.org/10/bs34dc, 2012.

Gurnis, M., Turner, M., Zahirovic, S., DiCaprio, L., Spasojevic, S., Müller, R. D., ... and Bower, D. J.: Plate tectonic reconstructions with continuously closing plates, Computers and Geosciences, 38(1), 35-42, 2012.

Gurnis, M., Mitrovica, J. X., Ritsema, J., and Heijst, H.-J. van.: Constraining mantle density structure using geological evidence of surface uplift rates: The case of the African Superplume, Geochemistry, Geophysics, Geosystems, 1(7), https://doi.org/10/ck4zt8, 2000.

Haq, B. U., J. Hardenbol, and P. R. Vail.: Chronology of fluctuating sea levels since the Triassic, Science, 235, 1156–1167, 1987.

Hassan, R., Williams, S. E., Gurnis, M., and Müller, R. D.: East African topography and volcanism explained by a single, migrating plume, Geoscience Frontiers, 11(5), 1669-1680, 2020.

Hu, J., Liu, L., Faccenda, M., Zhou, Q., Fischer, K. M., Marshak, S., and Lundstrom, C.: Modification of the Western Gondwana craton by plume–lithosphere interaction, Nature Geoscience, 11(3), 203, https://doi.org/10/gc6nb9, 2018.

Kounov, A., Niedermann, S., de Wit, M. J., Viola, G., Andreoli, M., and Erzinger, J.: Present denudation rates at selected sections of the South African escarpment and the elevated continental interior based on cosmogenic 3He and 21Ne, South African Journal of Geology, 110(2–3), 235–248, https://doi.org/10/fcx8hr, 2007.

Larsen, I. J., D. R. Montgomery, and Greenberg, H. M.: The contribution of mountains to global denudation, Geology, 42(6), 527–530, 2014.

Lithgow-Bertelloni, C., and Silver, P. G.: Dynamic topography, plate driving forces and the African superswell, Nature, 395(6699), 269–272, https://doi.org/10/fd5pfn, 1998.

Liu, L. and Gurnis, M.: Simultaneous inversion of mantle properties and initial conditions using an adjoint of mantle convection, Journal of Geophysical Research: Solid Earth, 113(B8), B08405, 2008.

Macgregor, D.: Understanding African and Brazilian Margin Climate, Topography and Drainage Systems, Implications for Predicting Deepwater Reservoirs and Source Rock Burial History, Search and Discovery Article #90100, 2010.

https://doi.org/10.5194/esurf-2021-89
Preprint. Discussion started: 8 December 2021

Macgregor, Duncan S.: Late Cretaceous–Cenozoic sediment and turbidite reservoir supply to South Atlantic margins, Geological Society, London, Special Publications 369.1 109-128, 2013.

Moucha, R., and Forte, A. M.: Changes in African topography driven by mantle convection, Nature Geoscience, 4(10), 707-712, 2011.

Müller, R. D., Hassan, R., Gurnis, M., Flament, N., and Williams, S. E.: Dynamic topography of passive continental margins and their hinterlands since the Cretaceous, Gondwana Research, 53, 225-251, 2018.

NOAA National Geophysical Data Center.: ETOPO1 1 Arc-Minute Global Relief Model. NOAA National Centers for Environmental Information. Accessed [17/06/2021] doi:10.7289/V5C8276M, 2009.

Nyblade, A. A., and Sleep, N. H.: Long lasting epeirogenic uplift from mantle plumes and the origin of the Southern African Plateau, Geochemistry, Geophysics, Geosystems, 4(12), https://doi.org/10/b6xqks, 2003.

Partridge, T. C., and Maud, R. R.: Geomorphic evolution of southern Africa since the Mesozoic, South African Journal of Geology, 90(2), 179–208, 1987.

Paul, J. D., Roberts, G. G., and White, N.: The African landscape through space and time, Tectonics, 33(6), 898–935, https://doi.org/10/f6ct3s, 2014.

Pérez-Gussinyé, M., Metois, M., Fernández, M., Vergés, J., Fullea, J., and Lowry, A. R.: Effective elastic thickness of Africa and its relationship to other proxies for lithospheric structure and surface tectonics, Earth and Planetary Science Letters, 287(1-2), 152-167, 2009.

Roberts, G. G., and White, N.: Estimating uplift rate histories from river profiles using African examples, Journal of Geophysical Research: Solid Earth, 115(B2), https://doi.org/10/b3wrqz, 2010.

Rouby, D., Bonnet, S., Guillocheau, F., Gallagher, K., Robin, C., Biancotto, F., ... & Braun, J.: Sediment supply to the Orange sedimentary system over the last 150My: An evaluation from sedimentation/denudation balance, Marine and Petroleum Geology, 26(6), 782–794, https://doi.org/10/bm25dp, 2009.

Salles, T. and Hardiman, L.: Badlands: An open-source, flexible and parallel framework to study landscape dynamics, Computers and Geosciences, doi:10.1016/j.cageo.2016.03.011, 2016.

Salles, T., X. Ding and G. Brocard.: pyBadlands: A framework to simulate sediment transport, landscape dynamics and basin stratigraphic evolution through space and time, PloS One, 13(4), doi:10.1371/journal.pone.0195557, 2018.

Scharf, T. E., Codilean, A. T., Wit, M. de, Jansen, J. D., and Kubik, P. W.: Strong rocks sustain ancient postorogenic topography in southern Africa, Geology, 41(3), 331–334, https://doi.org/10/f23vp5, 2013.

Stanley, J. R., Flowers, R. M., and Bell, D. R.: Kimberlite (U-Th)/He dating links surface erosion with lithospheric heating, thinning, and metasomatism in the southern African Plateau, Geology, 41, 1243– 1246, https ://doi.org/10.1130/G34797.1, 2013.

https://doi.org/10.5194/esurf-2021-89
Preprint. Discussion started: 8 December 2021

530 Tinker, J., de Wit, M., and Brown, R. W.: Linking source and sink: Evaluating the balance between onshore erosion and offshore sediment accumulation since Gondwana break-up, South Africa, Tectonophysics, 455(1–4), 94–103, https://doi.org/10/ctp34n, 2008a.

Tinker, J., de Wit, M., and Brown, R.: Mesozoic exhumation of the southern Cape, South Africa, quantified using apatite fission track thermochronology, Tectonophysics, 455, 77–93, https://doi.org/10.1016/j.tecto.2007.10.00, 2008b.

535 Wickert, A. D.: Open-source modular solutions for flexural isostasy: gFlex v1.0, Geoscientific Model Development, 9(3), 997–1017, doi:10.5194/gmd-9-997-2016, 2016.

Wildman, M., Brown, R., Watkins, R., Carter, A., Gleadow, A., and Summerfield, M.: Post break-up tectonic inversion across the southwestern cape of South Africa: New insights from apatite and zircon fission track thermochronometry, Tectonophysics, 654, 30–55, https://doi.org/10.1016/j.tecto.2015.04.012, 2015.

540 Wildman, M., Brown, R., Beucher, R., Persano, C., Stuart, F., Gallagher, K., ... & Carter, A.: The chronology and tectonic style of landscape evolution along the elevated Atlantic continental margin of South Africa resolved by joint apatite fission track and (U-Th-Sm)/He thermochronology, Tectonics, 35, 511–545, https ://doi.org/10.1002/2015T C004042, 2016.

Zhong, S.: Constraints on thermochemical convection of the mantle from plume heat flux, plume excess temperature, and upper mantle temperature, Journal of Geophysical Research: Solid Earth, 111(B4), 2006.

545